Characterizing Growth-Rate Dispersion of $NaNO_3$ Secondary Nuclei

Christopher M. Jones and Maurice A. Larson
Dept. of Chemical Engineering, Iowa State University, Ames, IA 50011

Previous work on growth-rate dispersion has shown how to calculate crystal-size distributions when the growth-rate distribution is known and how to calculate the growth rate distribution when the crystal-size distribution is known. There is a significant lack of information, however, on how growth-rate dispersion is affected by changes in system conditions like supersaturation, stirring speed, slurry density, or temperature. In this work, the growth-rate distributions of sodium nitrate secondary nuclei are characterized as a function of the nucleation and growing supersaturations. Growth-rate dispersion is characterized by analyzing the mean, spread, and shape of the growth-rate distribution. This provides a means of determining the factors that cause and control growth-rate dispersion. The analysis of this experimental work provides valuable insight into the relationships among supersaturation conditions, strain, and dislocation density. The average growth rates of secondary nuclei are dislocation controlled at low growing supersaturations and strain controlled at high growing supersaturations, where increasing the nucleation supersaturation causes an increase in both dislocation density and strain. Increasing strain by itself will decrease growth rates, while increasing dislocation density by itself will increase growth rates. This work also suggests that harsh system conditions can affect growth rates adversely.

Introduction

Growth-rate dispersion (GRD) was first recognized as a phenomenon that had a serious bearing on crystallizer performance in 1971 by White and Wright (1971). They observed that the standard deviation of an initially narrow size distribution of crystals in a batch crystallizer increased as time progressed. This meant that the crystals in their crystallizer were not growing at the same rate.

Early work first centered on defining and clarifying how GRD manifested itself in crystallization systems. A particular point of emphasis was the question of whether the growth rates of crystals fluctuated randomly, the random fluctuation (RF) model (Randolph and White, 1977), or whether they were constant for each crystal, the constant crystal growth (CCG) model (Ramanarayanan, 1982), where the growth rates of all the crystals in a system could be fit by a probability density distribution. Further work assuming the CCG model has shown how the growth-rate distribution of crystals in a mixed-suspension, mixed-product removal (MSMPR) crystallizer can be derived from the product size and vice versa distribution (Larson et al., 1985; Zumstein and Rousseau, 1987; Berglund and Larson, 1984). Recent work has virtually dismissed the notion of the RF model of GRD in favor of an intrinsic growth-rate (IGR) model. The proposed IGR model assumes that a crystal's growth rate does not fluctuate randomly but is intrinsic to each crystal in the system and may change as system parameters change. At any time during the crystallization process, the growth rates of crystals in the crystallizer system can be expressed as a growth-rate distribution.

While these research projects have helped define how GRD affects the CSD, virtually no work has been performed investigating how GRD is affected by system parameters such as supersaturation, stirring speed, or slurry density. No criteria have been established for defining GRD for a particular system. It is generally accepted that crystal growth rates are in-

Correspondence concerning this article should be addressed to C. M. Jones at his new address: Dow Chemical Co., 845 Building, Midland, MI 48642.

trinsic and can be fit by a probability distribution. Thus, it is proposed that defining the GRD of a system requires parameterizing the growth-rate distribution, specifically, in terms of its mean, standard deviation, coefficient of variation, and its symmetry.

It is the growth rates of nuclei that determine the final product-size distribution of a crystallizer. If a crystal nucleus is growing slowly, it will be washed out of the crystallizer before ever reaching a size large enough to contribute significantly to the final product mass. It is well known that it is the growth-rate dispersion of nuclei in MSMPR crystallizers that is ultimately responsible for the accumulation of small particles seen in the slurry CSD. In most crystallization systems, nucleation occurs at supersaturations much lower than those required to initiate primary nucleation, but secondary nucleation occurs at both high and low levels of supersaturation. It is secondary nuclei that are formed in MSMPR and seeded batch experiments. That is why secondary or contact nuclei are studied in this article.

The purpose of the work presented in this article is to characterize the GRD of secondary $NaNO_3$ nuclei as a function of supersaturation. Ultimately, the goals of this research are to further the general understanding of how crystals grow, to determine how changes in supersaturation affect GRD, and to understand, at a fundamental level, why those changes in supersaturation are having the effect they do. The development of a working knowledge that describes the relationship of GRD with respect to supersaturation will be helpful in a pragmatic sense and in choosing new directions of crystallization research.

Experimental Studies

Growth cell

The growth rates of secondary nuclei produced and grown under various levels of supersaturation were monitored. The cell used for secondary nucleation and growth was similar to that developed and used by Garside and Larson (1978) and is shown in Figure 1.

The cell had two chambers and consisted of four stainless-steel sections. The sections were separated by glass plates for the transmission of light from a microscope. Neoprene O-rings sealed the cell against fluid loss. The lower chamber had a volume of 8 mL, and it had an inlet and an outlet for the circulation of water from a Fisher Model 80 constant-temperature circulator. The upper chamber held the saturated solution and had a volume of 5 mL. The upper chamber also contained a thermocouple and the parent crystal mounted on a stainless-steel rod.

A Nikon Optiphot-2 microscope was used in coordination with a Javelin black-and-white digital video camera mounted on the microscope. Using a Corelco Oculus TCX/MX Frame Grabber and a Sony SVO-9500 MD VHS recorder, a run was taped for later image analysis. Image analysis was performed using Image Pro. Images were captured from the Fuji T-160 VHS tape, and the sizes of various nuclei were recorded.

Constant-temperature circulators were used to control the temperature of the cell. Nalgene tubing connected the water baths to the cell, and valves were used to control the flow from various constant-temperature baths.

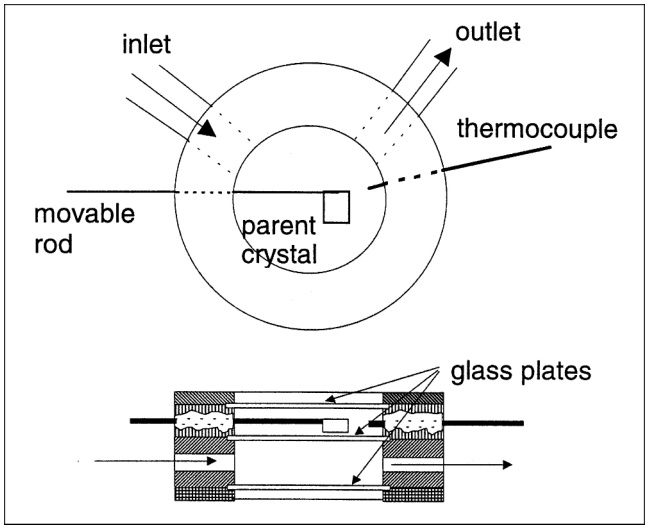

Figure 1. Growth cell used to observe secondary nuclei.

Materials and procedure

Saturated Solution. Analytical-grade $NaNO_3$ and distilled water were used to make the saturated solution. After mixing with a magnetic stirrer in an Erlenmeyer flask, the flask was put in a water bath at the desired temperature, making sure that a large excess of solid crystal still existed in the solution. The solution was considered saturated after having been in the bath for 5 days with excess crystal. Sodium nitrate was used for this work because it was easy to identify and measure the crystallographic faces.

Parent crystals were prepared by allowing saturated solution of the desired substance to evaporate over many days. Crystals were nucleated by primary nucleation. When the growing crystals reached a length of about 4–10 mm, they were removed from the solution and dried. The parent crystal was mounted in the cell using fast-setting epoxy to glue it to the movable stainless-steel rod.

Procedure. At the beginning of any run, the cell was preheated with water from one of the circulating water baths to a temperature about 1°C greater than the saturation temperature. This ensured that when saturated solution was added to the cell that it did not undergo primary nucleation. The cell was mounted on the stage of the microscope so that its position could be manipulated mechanically. Five mL of saturated solution was withdrawn from the flask and transferred to the upper chamber of the cell. A glass plate was then put over the upper chamber to prevent evaporation and to facilitate using the microscope. Using the microscope, the upper chamber was examined to determine whether any nucleation had occurred or if some other contamination existed, forcing the experiment to be stopped and restarted.

Once the existence of nuclei in the cell was shown to be negative, the flow of circulating water was changed to a second water bath with a lower temperature. Thus, the solution became supersaturated and the parent crystal endured a change from a dissolving environment to a growing environment.

When the temperature of the cell had reached steady state, the parent crystal was contacted by sliding it 2 cm across the glass plate. Contact nuclei were formed by this event. The progress of the run was recorded using a VHS recorder. Recording was started 2 s before the parent crystal was contacted. The cell temperature was recorded at intervals throughout the run.

Two sets of experiments were performed. The first set examined the GRD of specific faces of $NaNO_3$ when the supersaturation during nucleation and growth were the same. The second set of experiments examined the GRD of a characteristic dimension when the supersaturation during nucleation and growth were varied.

Measurements. Secondary nuclei were examined, and crystals were not selected for analysis if they exhibited any of the following:

- One whole edge was touching another crystal.
- It could not be distinguished from surrounding crystals.
- It appeared to be the joining of two smaller crystals.

The Miller indices for the sodium nitrate faces are given in Figure 2. The sodium nitrate crystal is normally a rhombahedron, thus a parallelepiped, which makes for the easy identification and measurement of specific crystallographic faces. In the first set of experiments the GRD of specific faces was compared.

Using Image Pro, the size of a characteristic dimension—the square root of the area of the 104 or $\bar{1}0\bar{4}$ face was measured and plotted with respect to time for selected crystals. Excel and JMP were used for data reduction and plotting various regression models.

In the first set of experiments the growth-rate distributions of the 113 face, the 014 face, and the characteristic dimension were determined, but only the data from the characteristic dimension analysis are included here. In the second set of experiments only the characteristic dimension was studied.

Experimental Parameters. The relative supersaturation, σ, for any given set of experimental conditions, was determined by using a plot of the solubility of sodium nitrate in water with respect to temperature. The relative supersaturation is found using Eq. 1,

$$\sigma = \frac{C - C_{eq}}{C_{eq}}, \tag{1}$$

where C is the concentration of the supersaturated solution in units of (g $NaNO_3$/100 g H_2O), and C_{eq}, with the same units, is the equilibrium concentration of the solution at the given temperature.

Experiment Set No. 1. In experiment Set No. 1 only one experimental variable existed, the supersaturation of the system, because the supersaturation present during nucleation and growth was the same. Table 1 shows the level of undercooling and the associated relative supersaturation for each run performed in Set No. 1. The initial growth rates of the characteristic dimension for 3181 nuclei were measured in this set.

For each set of conditions, the growth rate distributions of three dimensions were compared: the characteristic length, the 113 face, and the 014 face.

Experiment Set No. 2. This experiment was designed to decouple the effect of supersaturation at nucleation and during growth. Since the results of Set No. 1 showed nonlinear behavior in some of the response variables, it was thought that the second set of experiments should also allow for the detection of nonlinearity. To meet that end a response surface experiment was designed and carried out. Response surface experiments allow the analysis of curvature in a surface defined by two experimental parameters. In all cases, statistical significance was set to be at the 99% confidence level.

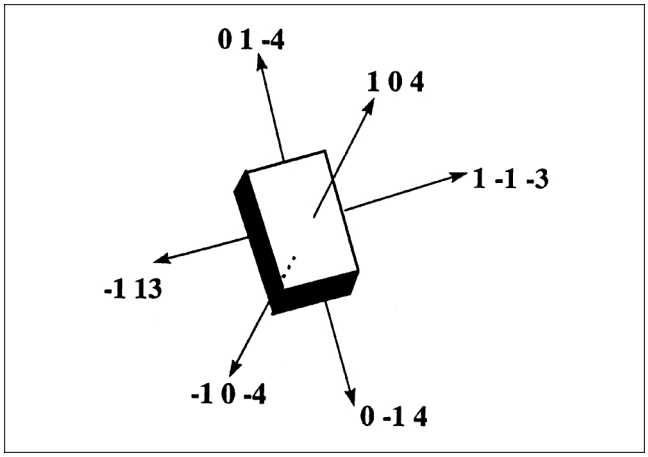

Figure 2. Miller indices for $NaNO_3$, a trigonal (hexagonal) system.

Relative supersaturation was determined the same way as in Set No. 1, where the concentration is defined in units of (g $NaNO_3$/100 g H_2O). The relative supersaturations were then coded; this allowed for statistical analysis without the possibility of collinearity between terms. The coded supersaturation was defined as,

$$X_{1,2} = \frac{2 \cdot (\sigma - 0.04127)}{0.02622}, \tag{2}$$

where X_1 is the coded supersaturation at nucleation, and X_2 is the coded supersaturation used when the crystal is growing. The coding was devised such that when $X = 1$, the relative supersaturation, corresponds with the highest level of supersaturation used in Set No. 1, or $\sigma = 0.05439$, and when $X = -1$, the relative supersaturation, corresponds with the lowest level of supersaturation used in Set No. 1, or $\sigma = 0.02816$.

The response surface design is shown in Table 2. The experiment included the measurement of the initial growth rates of 187 nuclei. Both the mean and the standard deviation of

Table 1. Supersaturation Conditions for Experimental Set No. 1

Run No.	ΔT °C	$\sigma = (C - C_{eq})/C_{eq}$	No. of Crystals Measured
1–2	3.3	0.028163	428
3–5	4.3	0.036835	679
6–8	5.2	0.044698	783
9–11	6.3	0.054387	1,291

Table 2. Experiment Set No. 2 Response Surface Design

Pattern	X_1	X_2	No. of Crystals Measured
−	−1	−1	20
+ −	1	−1	20
− +	−1	1	20
+ +	1	1	20
−0	−1.41421	0	20
+0	1.414214	0	20
0−	0	−1.41421	20
0+	0	1.414214	20
00	0	0	27

the initial growth-rate distributions were analyzed to determine their responses to X_1 and X_2.

However, the mean and standard deviation are analyzed differently. Because a distribution of standard deviations is skewed, the log of the standard deviation was fit. Taking the log of the standard deviation maps the skewed distribution into a form resembling a normal distribution. This allows for the correct statistical analysis, since detecting the statistical significance of a statistic is based upon the assumption that the statistic is normally distributed.

Results

While determining the growth rates of nuclei, it became immediately apparent that the growth rate changed as time progressed. That is, the measurements of nuclei size plotted with respect to time did not yield a linear fit in most cases. Instead the growth rate decelerated as time progressed. It is now thought that this deceleration is a result of the high ductility of sodium nitrate crystals. Sodium nitrate crystals subjected to tensile strain require a period of time in order for the strain to come to equilibrium within the crystal lattice (Ristic et al., 1997). Analogously, a recently formed nucleus would also by the very nature of its formation not be in equilibrium. It should be noted that in similar runs using potash alum and potassium sulfate, which are both more brittle than sodium nitrate, that they grew in a time-independent manner. Regardless of the cause of this phenomenon, it forced the fitting of a quadratic equation to the relationship between size and time:

$$S = at^2 + bt + c. \tag{3}$$

The growth rate at any time could then be found by taking the first derivative of Eq. 3:

$$G = 2at + b. \tag{4}$$

Since we are interested in describing the GRD behavior of nuclei, it became convenient to use the initial growth-rate distribution calculated at the nucleation event, where $t = 0$. The growth-rate distribution analysis had been complicated by the observed time-dependent growth rates of the secondary nuclei. In this analysis, the initial growth rate distribution is a distribution of the fitted parameter, b.

Experiment Set No. 1. The first set of experiments shows that the predicted response of the mean of the initial growth-rate distribution with respect to supersaturation is nonlinear. In this case the supersaturation at nucleation and during growth are the same. This is equivalent in the second experiment to setting X_1 and X_2 to be equal to each other.

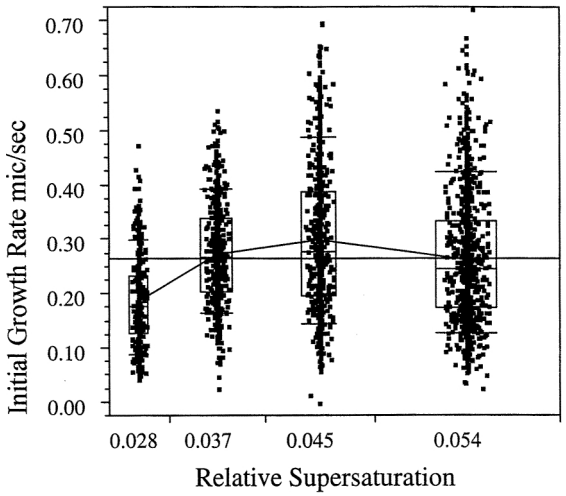

Figure 3. Set No. 1 results showing the initial growth rates at varying relative supersaturations.

The initial growth-rate distributions fit a gamma distribution. This is a skew-right distribution. Figure 3 shows the jittered distributions of the initial growth rates of the characteristic length of crystals by varying relative supersaturation. A line connects the means and the boxes surrounding the data points are quantile boxes. The jittering effect along with the quantile boxes is useful for getting a feel for the shape of the distribution at each set of experimental conditions. The growth-rate distributions are skew-right nonsymmetrical distributions and could be fit well with a gamma distribution.

Comparing the initial growth-rate distributions of specific faces at each set of conditions shows that there is no difference between the initial growth-rate distributions of the 113 face, the 014 face, or the characteristic length. This is as expected, since the faces of sodium nitrate are crystallographically equivalent. It is for this reason that only the data from the characteristic length are presented and only the characteristic length was studied in Set No. 2.

Statistical analysis of the data in Figure 3 results in the following predictive equations for the mean and standard deviation of the initial growth-rate distribution:

$$\mu = -0.514 + 36.3\sigma - 405\sigma^2 \tag{5}$$

$$\sigma_{IG} = \exp(-3.49 + 26.4\sigma). \tag{6}$$

Equation 5 predicts and Figure 3 shows that the response of the mean passes through a maximum. The spread of the distribution, measured by calculating the standard deviation and modeled in Eq. 6, increases with increasing supersaturation. The fitted response of the standard deviation in Eq. 6 is shown plotted with respect to the experimental values in Figure 4 where the points for Set No. 1 are represented by □.

The coefficient of variation (CV), which passes through a minimum with increasing supersaturation, is a measure of the

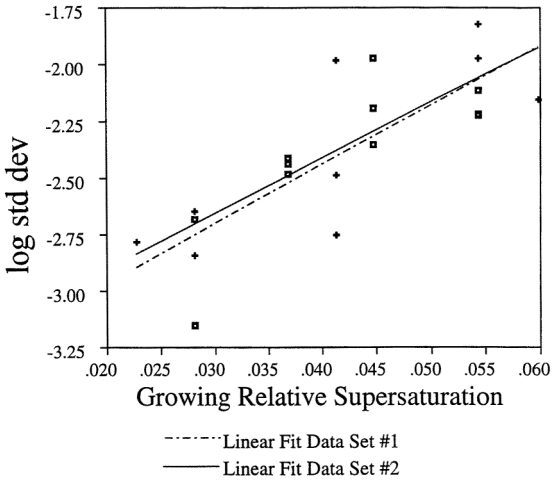

Figure 4. Plot of the log [standard deviation (μm/s) of initial growth rate distribution] with respect to the relative supersaturation during growth for Set No. 1 (□) and for Set No. 2 (+).

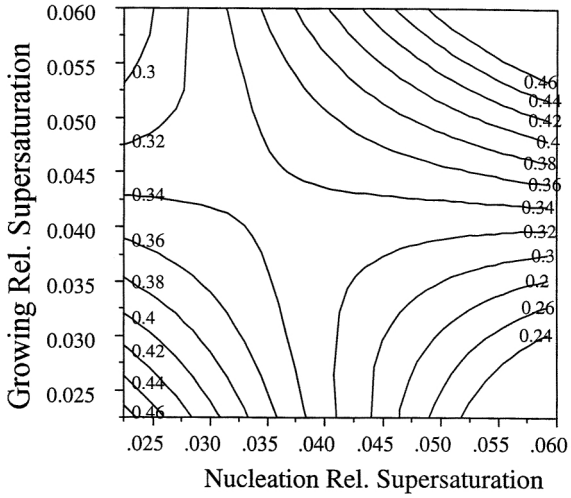

Figure 6. Contour plot of the coefficient of variation, CV, with respect to the relative supersaturation at nucleation, σ_1, and during growth, σ_2.

relative spread of the growth-rate distribution. The CV of the growth-rate distribution can be useful in the following way: if in a batch process, one started with a narrow size distribution of seed and wanted to have the spread of the CSD increase as little as possible, while having the highest possible growth rate, one would choose system conditions to minimize the CV.

The CV can be determined by dividing the standard deviation, Eq. 6, by the mean, Eq. 5, in Eq. 7:

$$CV = \frac{\sigma_{IG}}{\mu}. \tag{7}$$

Experimental Set No. 2. In Figure 5 the response surface of the mean initial growth rate is plotted on a contour plot

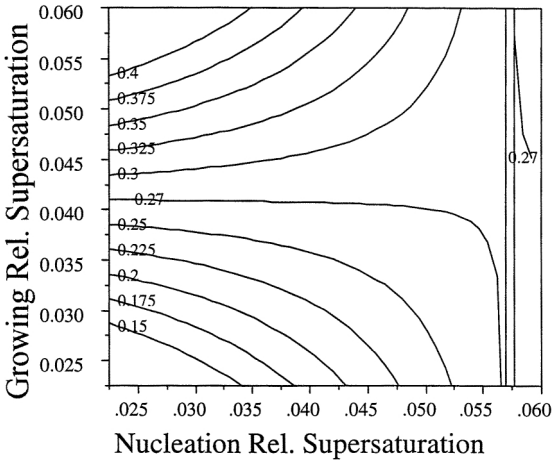

Figure 5. Contour plot of the mean of the initial growth-rate distribution as a function of relative supersaturation at nucleation, σ_1, and during growth, σ_2.

with respect to σ_1 and σ_2, the relative supersaturations at nucleation and growth. The lines of the contour plot represent different values of the mean, and the surface has a saddle point. The behavior of the mean of the initial growth-rate distribution is highly dependent upon both σ_1 and σ_2. Changing either the supersaturation conditions present during nucleation or growth can drastically alter the GRD behavior of the system.

The response surface analysis yields the following models, in terms of the relative supersaturations σ_1 and σ_2, for the mean and standard deviation of the initial growth-rate distribution after dropping statistically insignificant terms:

$$\mu = -0.415 + 16.8\sigma_2 - 292.66\sigma_1\sigma_2 + 12.08\sigma_1 \tag{8}$$

$$\sigma_{IG} = \exp(-3.39 + 24.6\sigma_2), \tag{9}$$

and again the CV can be calculated as in Eq. 7.

The model of the standard deviation is dependent only upon the supersaturation present during growth, σ_2. The relationship between growing supersaturation and the standard deviation is displayed in Figure 4. The solid line represents Eq. 9, and the points represented by the + are the calculated values of the standard deviation from Set No. 2.

Figure 6 shows the response of the coefficient of variation of the initial growth-rate distribution to σ_1 and σ_2 on a contour plot. Each line represents a different value of CV. The surface has a saddle point. The behavior of the CV is similar to that of the mean in that it is highly dependent upon both the nucleation and growing supersaturations. Altering the nucleation supersaturation can greatly alter the response of the CV to the growing supersaturation.

Comparing the Results of Set No. 1 and Set No. 2. By setting both σ_1 and σ_2 to be equal, the models derived in the analysis of Set No. 2 for the mean, standard deviation, and CV of the initial growth rate distribution can be compared to the models of Set No. 1 as shown in Figure 7.

The error bars are calculated using $\pm 3\times$(standard error), providing 99% confidence intervals for the fitted curves. The

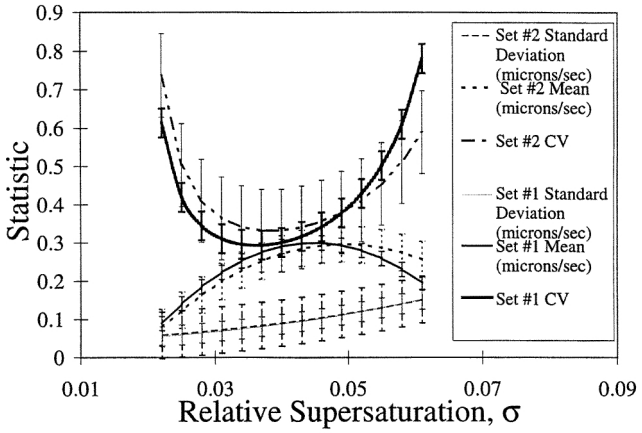

Figure 7. Comparison of the predicted response of the mean, standard deviation, and CV when the supersaturation at nucleation and during growth are the same for experiment Sets No. 1 and No. 2.

plots show there is good agreement between the two sets of experiments for the mean, standard deviation, and the CV.

Discussion

Experiment Set No. 1 showed that the initial growth rate distribution can be fit very well by a gamma distribution. In addition, comparisons of the initial growth-rate distributions of the characteristic length, the 113, and 014 faces showed that there was no detectable difference between them. This was as expected, because the faces of sodium nitrate are crystallographically equivalent. In the work of Berglund and Larson (1984) it was assumed that the growth-rate distribution used to determine the CSD was a gamma distribution. The results presented here support that assumption.

Experiment Set No. 1 showed that the standard deviation of the initial growth-rate distribution increased with increasing supersaturation, while the response of the mean passed through a maximum with increasing supersaturation. It was expected prior to these experiments that the mean would increase with increasing supersaturation, as most growth rate models would predict for a single crystal. This was not observed, because the mean is also a function of the nucleation supersaturation, which was being changed at the same rate as the growth supersaturation.

In their work, Ristic et al. (1991) showed that refacetting macrosized crystals at different supersaturations resulted in varying levels of dislocation density, where increasing the supersaturation increased the dislocation density. X-Ray topographs also showed that the area surrounding the seed crystal where the refacetting took place was highly strained. The logical jump was made that the formation of secondary nuclei was analogous to the refacetting of seed crystals, and that, as a result, increasing the supersaturation present during nucleation would increase both the dislocation density and the level of strain in those nuclei. A dislocation is by its very nature also a source of strain. That is why they show up as dark regions on an X-ray topograph.

Strain and dislocations have opposite effects on crystal growth rates. Ristic et al. (1991) working with macrosized potash alum crystals showed that increasing dislocation density results in increasing crystal growth rates. In separate experiments, but in the same article, they showed that increasing strain in macrosized potash alum crystals decreases the growth rates of the crystals. In addition, if the strain reached a critical level, the growth of the crystal could be stopped entirely until either the strain was released or the supersaturation was increased. It thus stood to reason that by the very nature of dislocations and strain, their effects on crystal growth rates were confounded. Experiment Set No. 2 was executed to separate and identify the elements of the main and interaction effects of both phenomena.

In experiment Set No. 2 the response of the standard deviation of the initial growth-rate distribution mimicked the behavior in Set No. 1. Set No. 2 showed that the standard deviation was dependent only upon the supersaturation present during growth. Changing the nucleation supersaturation had no effect on standard deviation.

In contrast, the mean of the initial growth-rate distribution was shown to be a function of both the nucleation and growth supersaturations. The behavior of the mean on the response surface was highly dependent upon what region of the response surface was being examined. Examining specific slices of the mean's response surface provides a way of clarifying and separating trends of the response surface with respect to strain and dislocation density, both of which are known to affect crystal growth rates.

Figure 8 shows the response of the mean of the initial growth-rate distribution with respect to increasing nucleation supersaturation at two levels of growing supersaturation. Increasing the nucleation supersaturation increases both the level of strain and the dislocation density. The mean increases with respect to increasing nucleation supersaturation at a low level of growing supersaturation, but decreases at a high level of growing supersaturation. This indicates two sep-

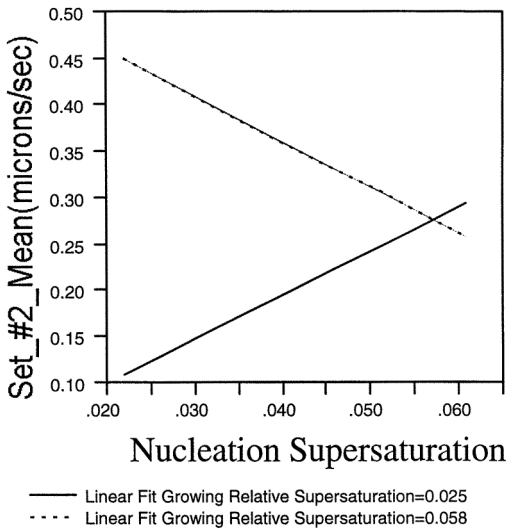

Figure 8. Response of the mean initial growth rate with respect to nucleation supersaturation at two levels of growing supersaturation.

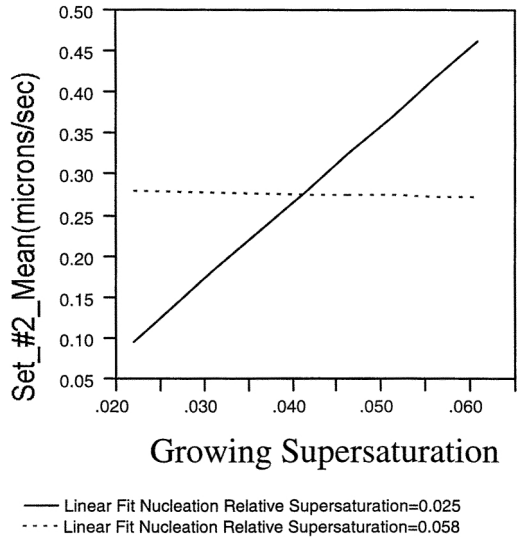

Figure 9. Response of the mean initial growth rate with respect to growing supersaturation at two levels of nucleation supersaturation.

arate regions of control. The first region at low-growing supersaturation is dislocation controlled, and the second region at high-growing supersaturations is strain controlled. As the growing supersaturation increases, crystal growth rates move from a dislocation-controlled growth to strain-controlled growth.

Zacher and Mersmann (1991), with MSMPR experiments using potash alum, showed that increasing the level of supersaturation in the crystallizer increased the level of strain and imperfections in the alum crystals. They also demonstrated that large crystals, or those with high growth rates, had the lowest levels of strain, while small crystals had the highest levels of strain. These results support the findings of Ristic et al. (1991) that increasing strain causes crystals to grow more slowly. Their work also supports the assertion that high levels of supersaturation increase the level of strain and imperfections in crystals.

Figure 9 shows the response of the mean of the initial growth-rate distribution with respect to increasing growing supersaturation at two levels of nucleation supersaturation. The mean increases with respect to increasing growing supersaturation at a low level of nucleation supersaturation, but the mean remains relatively constant at high levels of nucleation supersaturation. The results show that at low levels of strain, increasing the growing supersaturation increases the average growth rates of crystals in the system. At a critical level of nucleation supersaturation, the dislocation structure becomes such that increasing the growing supersaturation starts to decrease the average growth rate. Even though increasing the growing supersaturation will increase the growth rates of single crystals, the mean growth rate will actually start to decrease with increasing growing supersaturation if the nucleation supersaturation is high enough.

These results can be used to predict the effects of some other crystallizer variables on growth rates and growth-rate dispersion. Harsh conditions, such as high temperatures, high slurry density, high pressures, being passed through a pump, and high stirring speeds, will contribute to the level of strain and defects of crystals in a crystallizer. This results in lower crystal growth rates. Strain is a bulk effect changing the chemical potential of the crystal. This serves to reduce the driving force for growth. High supersaturation levels result in increased levels of the spread of the growth-rate distribution. This is undesirable when one wants a narrow CSD, especially in batch processes. In MSMPR crystallizers, the results indicate that operating at higher supersaturation levels will result in smaller crystals in the CSD due to the increase in strain.

When comparing the results of Set No. 1 and Set No. 2 in Figure 7, the results match up very well with one another. The response of the standard deviation is almost the same. The modeled response of the mean for both sets predicts that a maximum will occur with increasing supersaturation. This maximum is a result of the complicated dependency of the mean upon both the nucleation and growing supersaturations. The CV or relative spread allows for comparing the spreads of distributions with different means. The coefficient of variation for both sets passes through a minimum and match up well with one another. It is also worth noting that Set No. 1 and Set No. 2 were performed a year and a half apart, and that the crystal measurements were performed by two different individuals. Still, the results match up very well, which adds to the validity of the results.

Conclusions

The initial growth-rate distribution is fit well by a gamma distribution. The responses of the mean, standard deviation, and CV of the initial growth-rate distribution have been found with respect to the supersaturation present during nucleation and growth. The mean and coefficient of variation of the initial growth-rate distribution are dependent upon both supersaturation at nucleation and supersaturation during growth. The standard deviation of the initial growth-rate distribution is dependent only upon the supersaturation present during growth. The general trends of the mean and standard deviation of the initial growth-rate distribution are displayed in Table 3.

The average growth rate the sodium nitrate secondary nuclei is dislocation controlled at low-growing supersaturations, and is strain controlled at high-growing supersaturations. Both dislocation density and strain increase with increasing levels of nucleation supersaturation, but the enhancement of crystal growth rates due to increases in dislocation density disappear as growing supersaturation increases.

It follows from this that other system conditions may contribute to the strain and dislocation density of crystals growing in a system, and that subjecting crystals to harsh conditions like grinding, high temperatures, high pressures, or im-

Table 3. Trends of the Initial Growth-Rate-Distribution with Varying Conditions of Supersaturation

Nucl. Supersat.	Growing Supersat.	Init. Growth-Rate Mean	Init. Growth-Rate Std. Dev.
Increases	Increases	Varies	Increases
Increases	Decreases	Varies	Decreases
Decreases	Fixed	Increases	Constant
Fixed	Decreases	Varies	Decreases

pact will cause a decrease in the average growth rate of crystals in the system.

The results of the two sets were reproducible. The two sets of experiments were performed one and half years apart, with the measurements performed by two different people.

Acknowledgments

The authors are grateful to Wayne Genck of Genck International for his financial support and to Seth Holmen, who worked as an undergraduate research assistant on experiment Set No. 1.

Notation

S = characteristic length, μm
t = time (s)

Literature Cited

Berglund, K. A., and M. A. Larson, "Modeling of Growth Rate Dispersion of Citric Acid Monohydrate in Continuous Crystallizers," *AIChE J.*, **30**, 280 (1984).

Garside, J., and M. A. Larson, "Direct Observations of Secondary Nuclei," *J. Cryst. Growth*, **43**, 694 (1978).

Larson, M. A., E. T. White, K. A. Ramanarayanan, and K. A. Berglund, "Growth Rate Dispersion in MSMPR Crystallizers," *AIChE J.*, **31**, 90 (1985).

Ramanarayanan, K. A., "Production and Growth of Contact Nuclei," PhD Diss., Iowa State Univ. of Science and Technology, Ames (1982).

Randolph, A. D., and E. T. White, "Modeling Size Dispersion in the Prediction of Crystal Size Distribution," *Chem. Eng. Sci.*, **32**, 1067 (1977).

Ristic, R. I., J. N. Sherwood, and T. S. Shripathi, "The Influence of Tensile Strain on the Growth of Crystals of Potash Alum and Sodium Nitrate," *J. Cryst. Growth*, **179**, 194 (1997).

Ristic, R. I., J. N. Sherwood, and T. S. Shripathi, "The Role of Dislocations and Mechanical Deformation in Growth Rate Dissipation in Potash Alum Crystals," *Advances in Industrial Crystallization*, Butterworth-Heinemann, Oxford, p. 77 (1991).

White, E. T., and P. G. Wright, "Magnitude of Size Dispersion Effects in Crystallization," *CEP Symp. Ser.*, **67**(110), 81 (1971).

Zacher, U., and A. Mersmann, "The Influence of Internal Crystal Perfection on Growth Rate Dispersion in a Continuous Suspension Crystallizer," *J. Cryst. Growth*, **147**, 172 (1995).

Zumstein, R. C., and R. W. Rousseau, "GRD in Batch Crystallization with Transient Conditions," *AIChE J.*, **33**, 1921 (1987).

Manuscript received Jan. 18, 1999, and revision received July 1, 1999.